

Supporting Information

Extreme Conductance Suppression in Molecular Siloxanes

Haixing Li,^{‡1} Marc H. Garner,^{‡2} Timothy A. Su,^{‡3} Anders Jensen,² Michael S. Inkpen,¹ Michael L. Steigerwald,^{*3} Latha Venkataraman,^{*1,3} Gemma C. Solomon,^{*2} Colin Nuckolls^{*3}

¹Department of Applied Physics and Applied Mathematics, Columbia University, New York, New York 10027, United States

²Nano-Science Center and Department of Chemistry, University of Copenhagen, Universitetsparken 5, 2100 Copenhagen Ø, Denmark

³Department of Chemistry, Columbia University, New York, New York 10027, United States

[‡] contributed equally

Table of Contents

I. Additional Figures.....	2
II. Synthetic Procedures and Characterization of Compounds.....	4
III. Computational Details.....	7
A: Building junctions in ASE	7
B: Siloxane conformations	8
D: HOMO-LUMO gap and sulfur orbital splitting	16
E: Complex band structure.....	18
IV. NMR Spectra (¹H, ¹³C, ²⁹Si):	20
V. References	26

I. Additional Figures

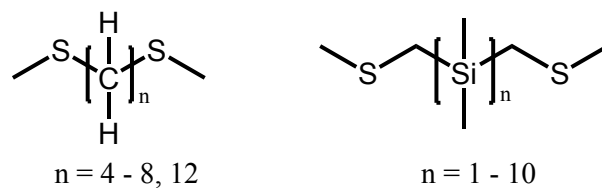


Figure S1. Chemical structures of linear alkanes and silanes.

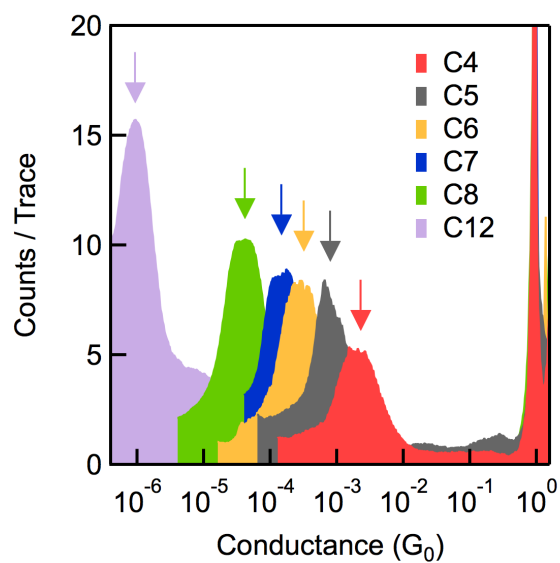


Figure S2. Conductance histograms for alkanes.

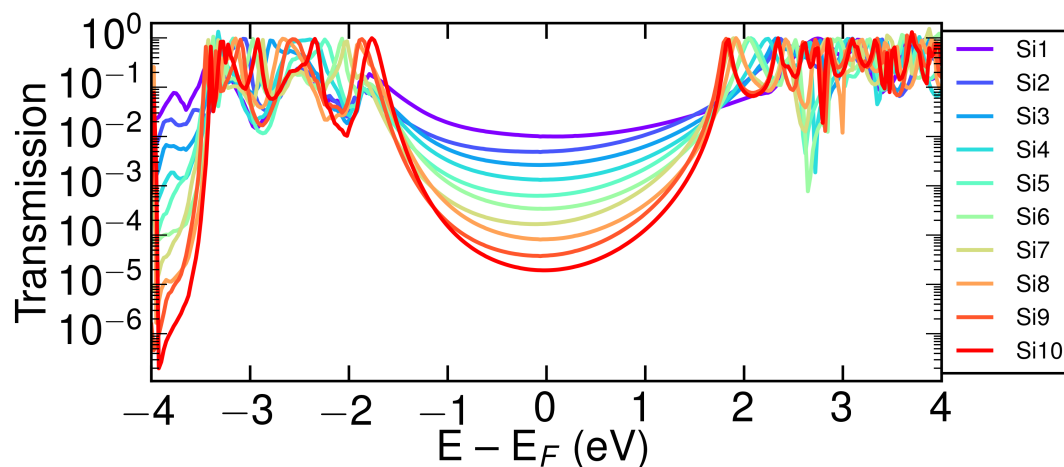


Figure S3. Transmission curves for linear silanes **Si1** - **Si10**.

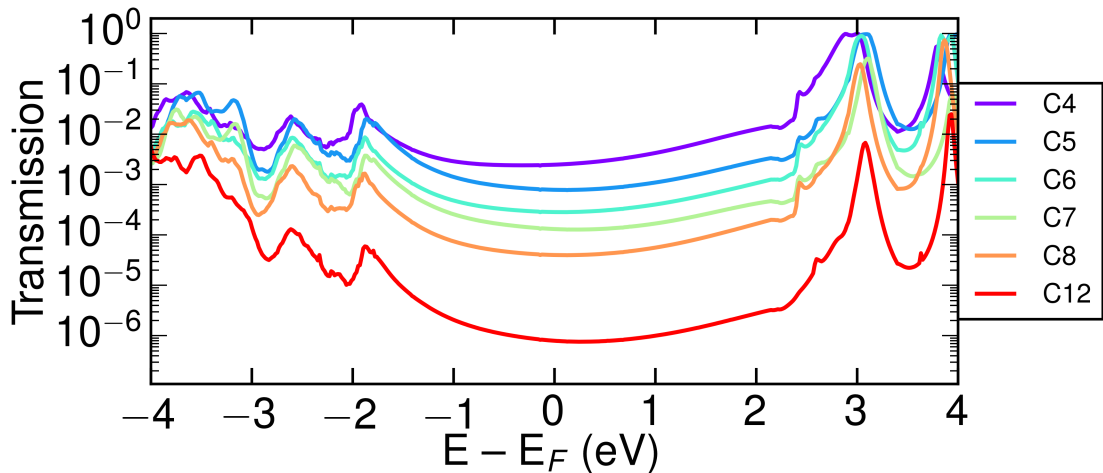


Figure S4. Transmission curves for linear alkanes C₄-C₈ and C₁₂.

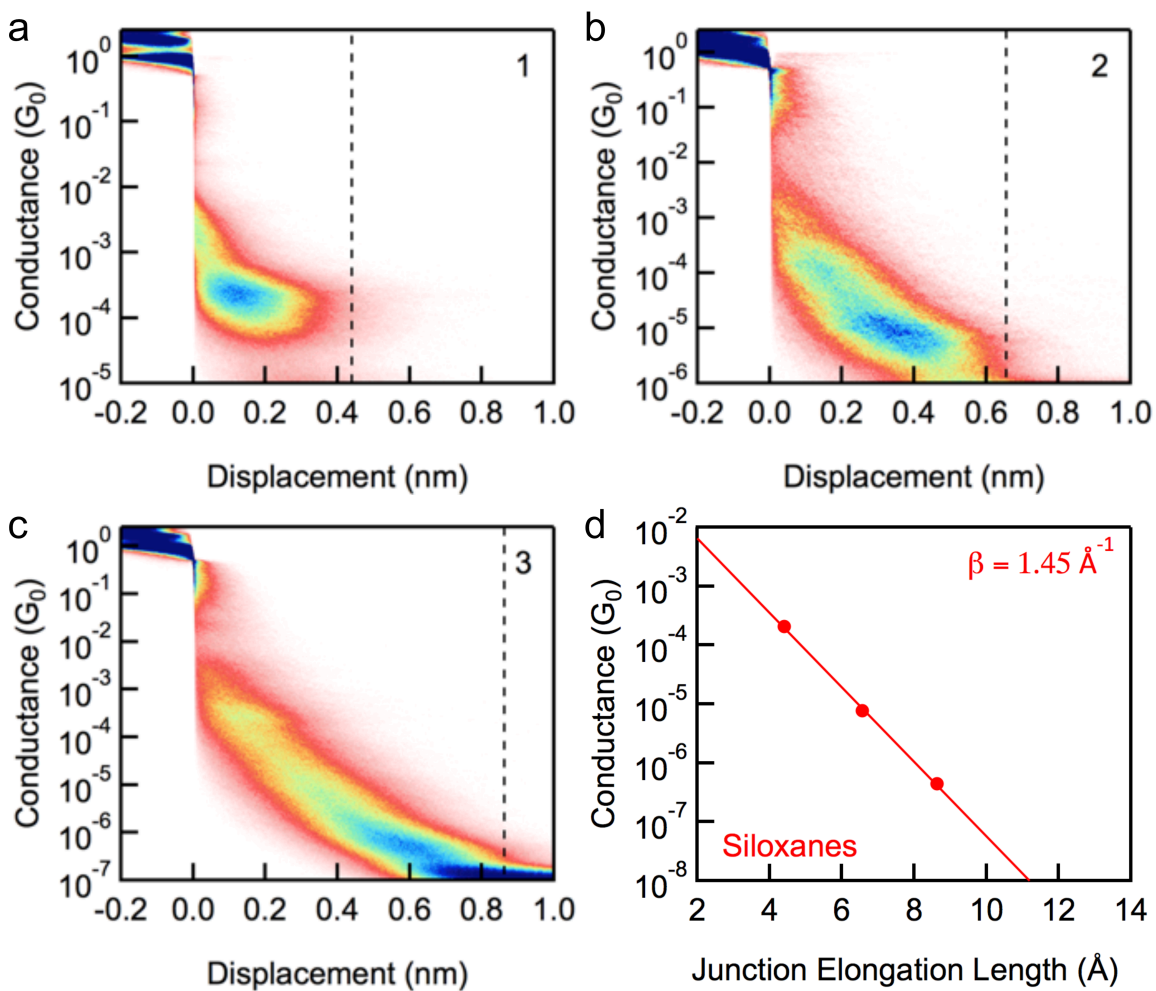


Figure S5. (a)-(c) 2D conductance histograms of **1-3** by aligning all the traces at the point where the conductance crosses $0.5G_0$ and then overlaying them. The vertical dashed lines indicate the junction elongation length, defined as the distance when the conductance distribution drops to 20% of its peak value for each molecule measured. (d) Plot of the conductance as a function of the junction elongation length, defined as the 80 percentile length from the 2D conductance histograms, for **1-3**. Using $G = G_0 e^{-\beta L}$, we determine a decay constant of $1.45 \pm 0.04 \text{ \AA}^{-1}$ for siloxanes.

II. Synthetic Procedures and Characterization of Compounds

All reactions were performed in oven-dried or flame-dried round bottom flasks, unless otherwise noted. The flasks were fitted with rubber septa and reactions were conducted under a positive pressure of nitrogen or argon unless otherwise noted. Anhydrous and anaerobic solvents were obtained from a Schlenk manifold with purification columns packed with activated alumina and supported copper catalyst (Glass Contour, Irvine, CA). Automated flash chromatography was performed using a Teledyne Isco Combiflash R_f200 and Rediseq R_f Gold Silica columns.

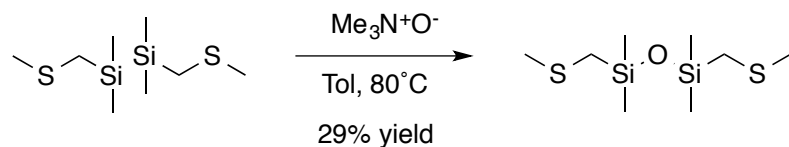
Materials. Commercial reagents were used without further purification unless otherwise noted. Trimethylamine N-oxide was purchased from Sigma-Aldrich. The α,ω -bis(thiomethyl)permethyloligosilanes (**Si₂-CSMe**, **Si₃-CSMe**, and **Si₄-CSMe**) were synthesized according to previously reported methods.¹

Instrumentation. ¹H, ¹³C, and ²⁹Si NMR spectra were recorded on a Bruker DRX300 (300 MHz), Bruker DRX400 (400 MHz) or a Bruker DMX500 (500 MHz) spectrometer. Chemical shifts for protons are reported in parts per million downfield from tetramethylsilane and are referenced to residual protium in the NMR solvent (CHCl₃: δ 7.26). Chemical shifts for carbon are reported in parts per million downfield from tetramethylsilane and are referenced to the carbon resonances of the solvent (CDCl₃ δ 77.16). Chemical shifts for silicon are reported in parts per million downfield from tetramethylsilane and referenced to the silicon resonance of tetramethylsilane (TMS δ 0.0). The silicon NMR resonances were determined with a DEPT pulse sequence. Data are represented as follows: chemical shift, multiplicity (s = singlet, d = doublet, dd = doublet of doublets, t = triplet, m = multiplet), coupling constants in Hertz, and integration. The mass spectroscopic data were obtained at the Columbia University mass spectrometry facility using a Waters XEVO G2XS QToF mass spectrometer equipped with a UPC2 SFC inlet,

electrospray ionization (ESI) probe, atmospheric pressure chemical ionization (APCI) probe, and atmospheric solids analysis probe (ASAP+).

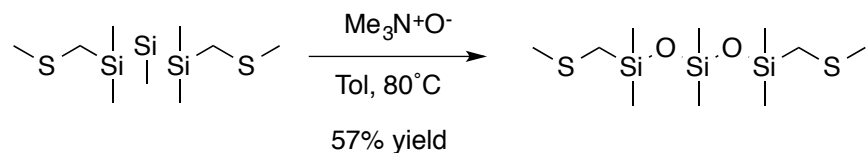
Synthetic Details

[SiO]₁



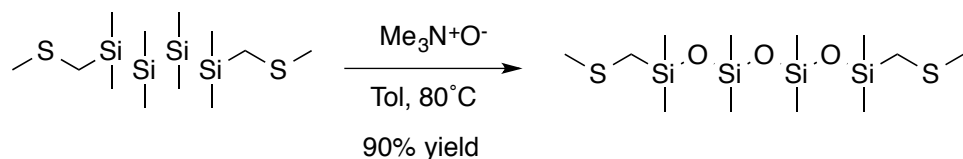
1,2-bis(thiomethyl)tetramethyldisilane (58 mg, 0.243 mmol, 1.00 equiv.) was added to a 20 mL scintillation vial equipped with a stir bar. Trimethylamine N-oxide (36 mg, 0.486 mmol, 2.00 equiv.) was added to the vial, followed by 5 mL toluene. The reaction mixture was stirred at 80°C for 2 hours. The solvent was removed *in vacuo*. The crude material was dissolved in a 7:3 hexanes:dichloromethane solvent mixture, passed through an Al₂O₃ plug, then concentrated to give a pale yellow oil (18 mg, 29% yield). ¹H NMR (500 MHz, CDCl₃) δ 2.16 (s, 6H), 1.81 (s, 4H), 0.18 (s, 12H). ¹³C NMR (126 MHz, CDCl₃) δ 22.53, 20.17, 0.37. ²⁹Si NMR (60 MHz, CDCl₃) δ 4.48. HRMS (TOF MS ASAP+) for C₈H₂₂OS₂Si₂H ([M+H]⁺): calculated = 255.0729, found = 255.0715.

[SiO]₂



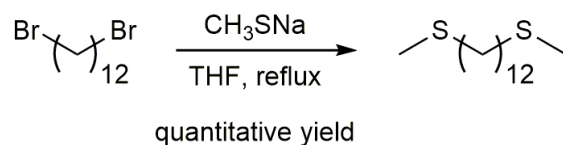
1,3-bis(thiomethyl)hexamethyltrisilane (43 mg, 0.145 mmol, 1.00 equiv.) was added to a 20 mL scintillation vial equipped with a stir bar. Trimethylamine N-oxide (44 mg, 0.580 mmol, 4.00 equiv.) was added to the vial, followed by 5 mL toluene. The reaction mixture was stirred at 80°C for 2 hours. The solvent was removed *in vacuo*. The crude material was dissolved in a 7:3 hexanes:dichloromethane solvent mixture, passed through an Al₂O₃ plug, then concentrated to give a colorless oil (27 mg, 57% yield). ¹H NMR (500 MHz, CDCl₃) δ 2.15 (s, 6H), 1.81 (s, 4H), 0.19 (s, 12H), 0.08 (s, 6H). ¹³C NMR (126 MHz, CDCl₃) δ 22.50, 20.16, 1.33, 0.27. ²⁹Si NMR (60 MHz, CDCl₃) δ 3.39, -19.46. HRMS (TOF MS ASAP+) for C₁₀H₂₈O₂S₂Si₃H ([M+H]⁺): calculated = 329.0917, found = 329.0917.

[SiO]₃



1,4-bis(thiomethyl)octamethyltetrasilane (71 mg, 0.199 mmol, 1.00 equiv.) was added to a 20 mL scintillation vial equipped with a stir bar. Trimethylamine N-oxide (90 mg, 1.19 mmol, 6.00 equiv.) was added to the vial, followed by 4 mL toluene. The reaction mixture was stirred at 80 °C for 2 hours. The solvent was removed *in vacuo*. The crude material was dissolved in a 7:3 hexanes:dichloromethane solvent mixture, passed through an Al₂O₃ plug, then concentrated to give a colorless oil (72 mg, 90% yield). ¹H NMR (500 MHz, CDCl₃) δ 2.15 (s, 6H), 1.81 (s, 4H), 0.19 (s, 12H), 0.08 (s, 12H). ¹³C NMR (126 MHz, CDCl₃) δ 22.49, 20.13, 1.28, 0.27. ²⁹Si NMR (99 MHz, CDCl₃) δ 3.51, -20.49. HRMS (TOF MS ASAP+) for C₁₂H₃₄O₃S₂Si₄H ([M+H]⁺): calculated = 403.1105, found = 403.1094.

C12



The synthesis of **C12** was adapted from literature methods.² 1,12-Dibromododecane (0.523 g, 1.59 mmol) and sodium thiomethoxide (0.30 g, 4.3 mmol) were added to a round bottomed flask equipped with a stirrer bar and condenser. THF (10 mL) was added and the mixture refluxed with stirring overnight. The mixture was cooled to room temperature and solvent removed *in vacuo*. After extraction into CH₂Cl₂ and filtration through a silica plug, the crude product was preabsorbed on silica and loaded on a silica column packed with hexanes. Elution with 0-20% CH₂Cl₂ in hexanes provided **C12** as a low melting point white solid (0.415 g, quantitative yield). *Note:* TLC plates were stained using basic KMnO₄. ¹H NMR (400 MHz, CDCl₃) δ 2.48 (t, *J* = 7.4 Hz, 4H), 2.09 (s, 6H), 1.58 (m, 4H), 1.42-1.22 (m, 16H). ¹³C{¹H} NMR (101 MHz, CDCl₃) δ 34.46, 29.72, 29.67, 29.41, 29.34, 28.99, 15.70. HRMS (TOF MS ASAP+) for C₁₄H₃₀S₂ ([M+H]⁺): calculated = 263.1867, found = 263.1868.

III. Computational Details

A: Building junctions in ASE

This section briefly describes the systematic procedure we use to build single-molecule junctions in the atomic simulation environment (ASE).

Following optimization in vacuum as described in the manuscript, single-molecule junctions are built using the following procedure:

1. The optimized conformation of the molecule is loaded into the ASE software. The molecule must be in a conformation where the terminal Si-CH₂-S-CH₃ dihedrals are in *ortho*-configuration ($\sim 90^\circ$). For alkanes the terminal CH₂-CH₂-S-CH₃ dihedral must be in a *gauche* conformation ($\sim 70^\circ$).
2. Single gold atoms are placed in the positions where we expect the tips of the electrodes to be. On the basis of test-calculations, we use the following starting-parameters (these will be the starting point for the relaxation).

For siloxanes and silanes:

- S-Au bond-length: 2.525 Å
- C-S-Au bond angle: 110°
- Si-CH₂-S-Au dihedral: $\pm 170^\circ$

For Alkanes:

- S-Au bond-length: 2.525 Å
- C-S-Au bond angle: 110°
- CH₂-CH₂-S-Au dihedral: 180°

3. The molecule with tip gold atoms is placed on 4x4x4 fcc111 gold slab with a three-atom plateau on it, which in combination with the tip gold atom forms a four-atom pyramid (a tetrahedron).
4. The tip gold atom axis is aligned with the junction z-axis (the direction of the current), and a three-atom plateau is placed on the other side as well. By using periodic boundary conditions in all directions, the molecule is placed between two four-atom pyramids on Au-surfaces as can be seen in Figure S6.

The junction is relaxed to a force threshold of 0.05 eV/Å for all atoms, with the gold atoms kept fixed. Two k-points are sampled in the irreducible part of the Brillouin zone. A second gold slab completes the junction as periodic boundary conditions are not used in the transport direction when the transmission is calculated. Finally, the Landauer transmission is calculated using the non-equilibrium Green's functions approach. Eight k-points are sampled in the irreducible part of the Brillouin zone for the transport calculation.

conformation where dihedrals alternate between *transoid* and *syn* dihedrals along the molecular backbone (see fig. 2a in the manuscript). We note that these resemble conformations seen in simulations of siloxane polymer stretching experiments.^{11,12} In agreement with the literature, we find the Si-O-Si bond angles to be very flexible. This is highlighted in Figure S7, where the Si-O-Si bond angles of Siloxane 1 and Siloxane 2 are manipulated without further optimization. The bond angles can almost extend to a linear conformation with an energy penalty of only a few kT at room temperature (~ 0.026 eV).

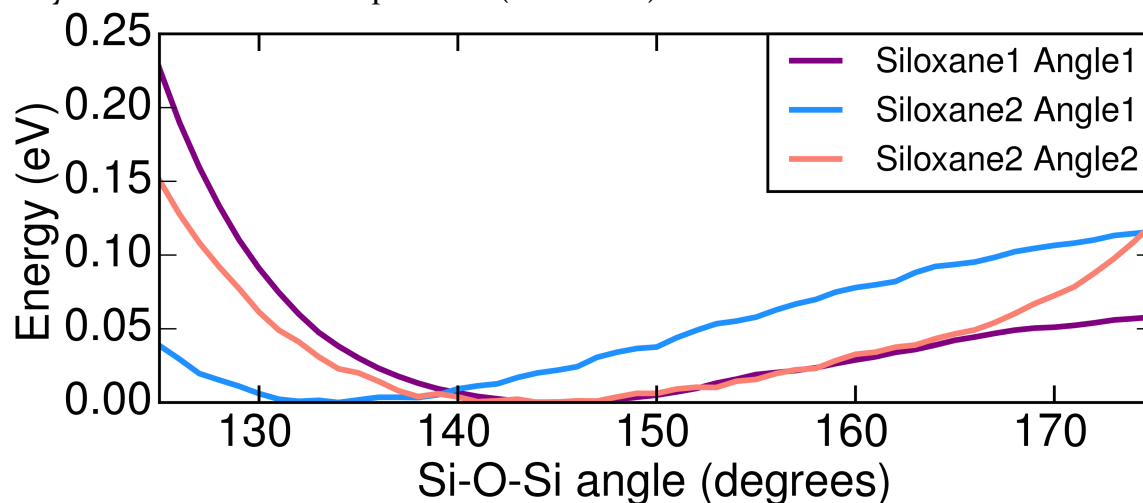


Figure S7. Total energy of siloxane 1 and siloxane 2 where the Si-O-Si bond angle is varied. The energy zero is set to that of the optimized structure.

As a consequence of the shallow potential energy surface there are alternative conformations to the alternating *syn-transoid* conformations that are also low—and slightly lower—in energy. We shall briefly review these and the effect it has on transmission and its decay with increasing molecular length. Conformations will be described by their dihedral angles along the backbone from the first $\text{CH}_2\text{-Si-O-Si}$ dihedral to the last Si-O-Si-CH_2 dihedral. *t* is transoid ($>150^\circ$) and *s* is syn ($<30^\circ$).

Siloxane 1

The *t-t* and *t-s* conformations are shown in Figure S8. The *t-t* conformation is 0.013 eV more stable, around half kT at room temperature. Like the energy difference, the difference in transmission is almost negligible close to the Fermi energy, as shown in Figure S8c. The junction of *t-t* is almost one Ångström shorter than *t-s*.

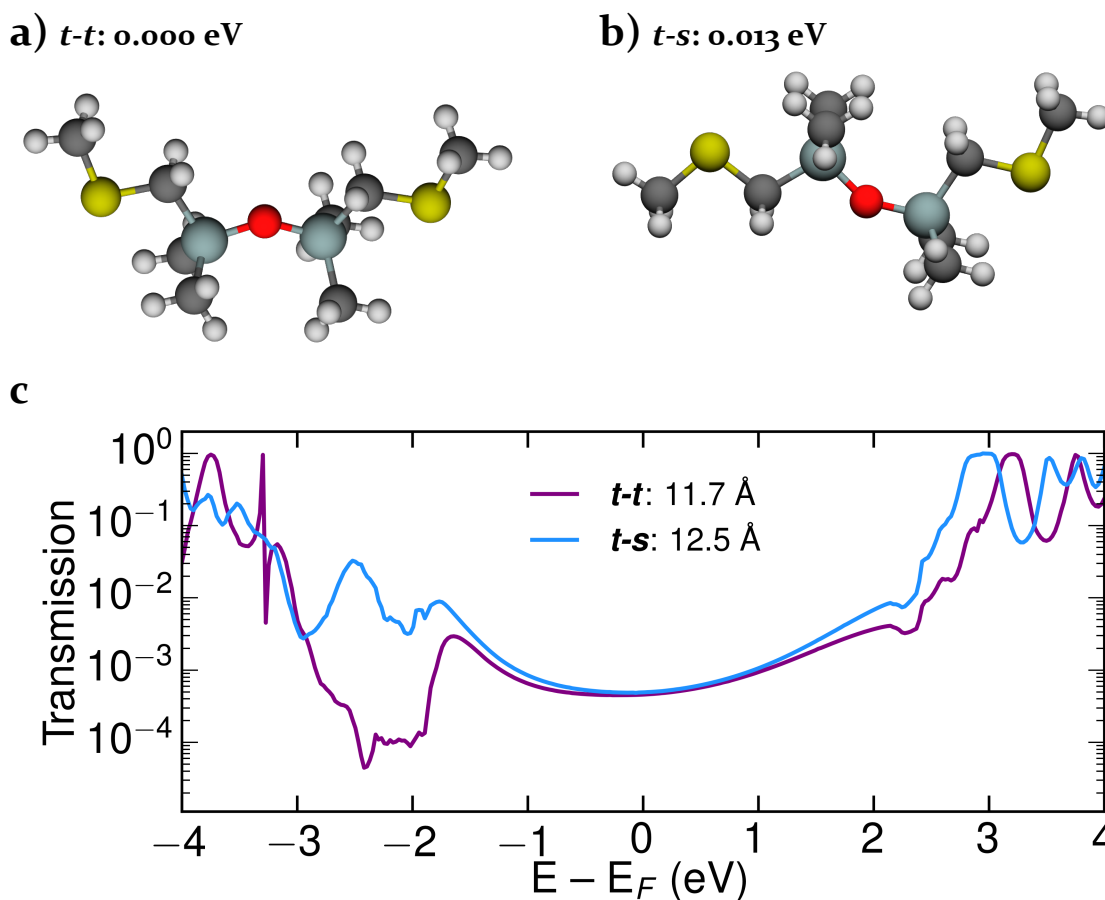
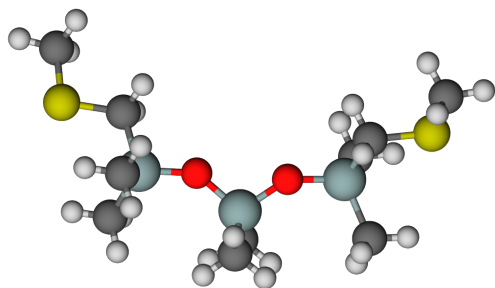


Figure S8. ab) Optimized vacuum conformations of siloxane **1** and energy relative to the most stable conformation. c) transmission plotted semilogarithmically against energy. Junction tip-to-tip Au-Au length is listed.

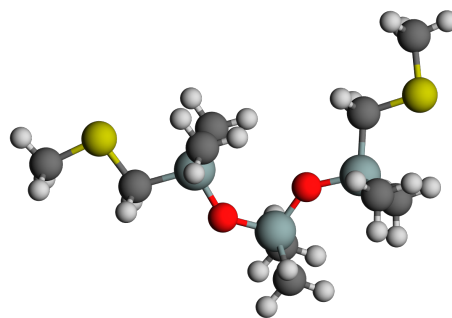
Siloxane **2**

For siloxane **2**, the all-*transoid* (Fig. S9a *t-t-t-t*) conformation is high in energy. Conformations with one or two *syn* dihedrals are low in energy, with the alternating *transoid-syn* conformation being around half kT at room temperature higher than *t-s-t-t* as shown in Figure S9bc. While the junction length differs by around two Ångströms, the transmission around the Fermi energy is almost unaffected by the conformational freedom of the molecule as shown in Figure S8d.

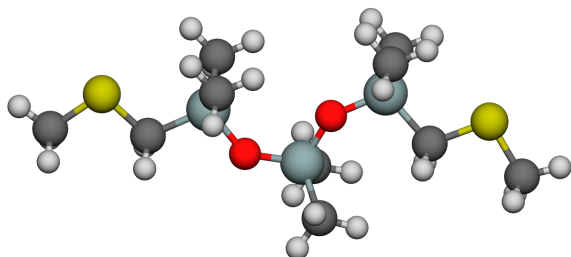
a) *t-t-t-t*: 0.076 eV



b) *t-s-t-t*: 0.000 eV



c) *t-s-t-s*: 0.014 eV



d)

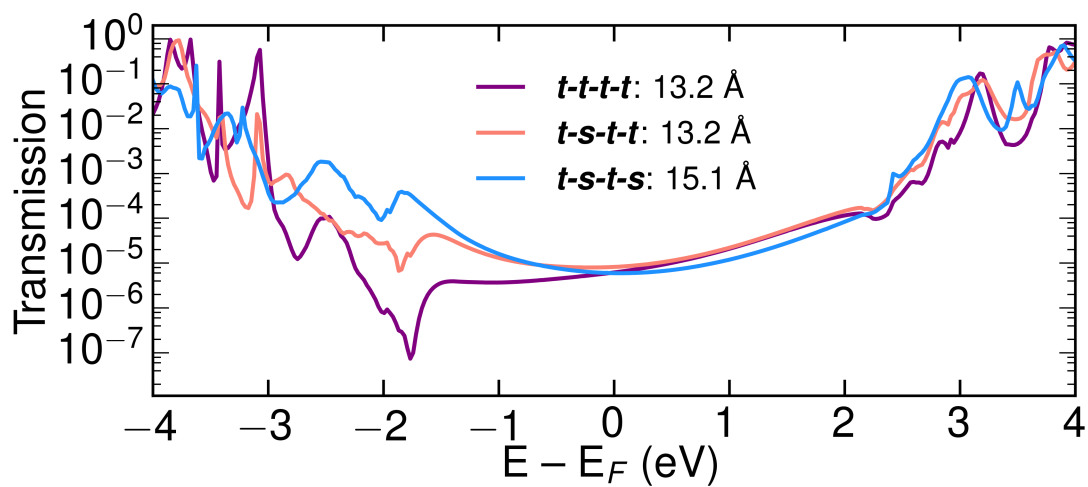


Figure S9. abc) Optimized vacuum conformations of siloxane **2** and energy relative to the most stable conformation. d) transmission plotted semilogarithmically against energy. Junction tip-to-tip Au-Au length is listed.

Siloxane 3

For siloxane 3, the all-*transoid* (Fig. S10a *t-t-t-t-t*) conformation is further higher in energy, and is unlikely to contribute to the experiments. Various conformations can be made with multiple *syn* dihedrals and are low in energy. These are shown in Figure S10bc and have a relative short structure, due to the bent conformation of the molecule. Still the sulfurs at the end are pointing along the length-axis of the molecule, so these may be likely to contribute in the experiment to some extent. The alternating *transoid-syn* conformation is still around half kT at room temperature higher in energy than the most stable conformation, and is shown in Figure S10d. The junction length of the bent conformations is around two Ångströms shorter than the *t-s-t-s-t-s* conformation, and consequently, the transmission around the Fermi energy is around an order of magnitude higher around the Fermi energy as shown in Figure S10e. The higher transmission is most likely due to the bent structure of the molecule, which may allow through-space coupling short-circuit the through-bond path.

Conformational freedom and decay of transmission

It is imperative that we understand how the conformational freedom affect the exponential decay factor, both in transmission calculations and experimental result because we use the effective molecular length (C-C linker distance) to calculate the experimental conductance exponential decay factor.

In figure S11, the transmission decay plots are shown as function of effective molecular length and number of atoms in the backbone for three siloxane series. Plotting against effective molecular length (left panel) shows that the decay of the all-*transoid* series is very high as the molecular length is shorter, while the transmission is largely the same as the alternating-*transoid-syn* series. The non-systematic series of most stable conformations (see Figs. S8-10) has a slightly smaller decay factor, still higher than the experimental factor. Plotting against number of atoms reveals that the decay factor per number of atoms is the same for the all-*transoid* and alternating-*transoid-syn* series, but smaller for the most stable series. This is consistent with that the most stable conformation of siloxane 3 (*s-t-s-s-t-s*) is bent and therefore through-space transmission may short-circuit the backbone of the molecule. It is indeed the third data-point that appears to fall of the trend-lines of the points of the other two series. Using the effective molecular length of the most stable conformations to calculate the experimental conductance exponential decay factor will result in a higher decay factor than the one we report in the manuscript, which will give better agreement with theory. Still, it is worth

noting that the conductance point of siloxane **3** does not fall significantly off the trend-line in Figure 1c of the manuscript.

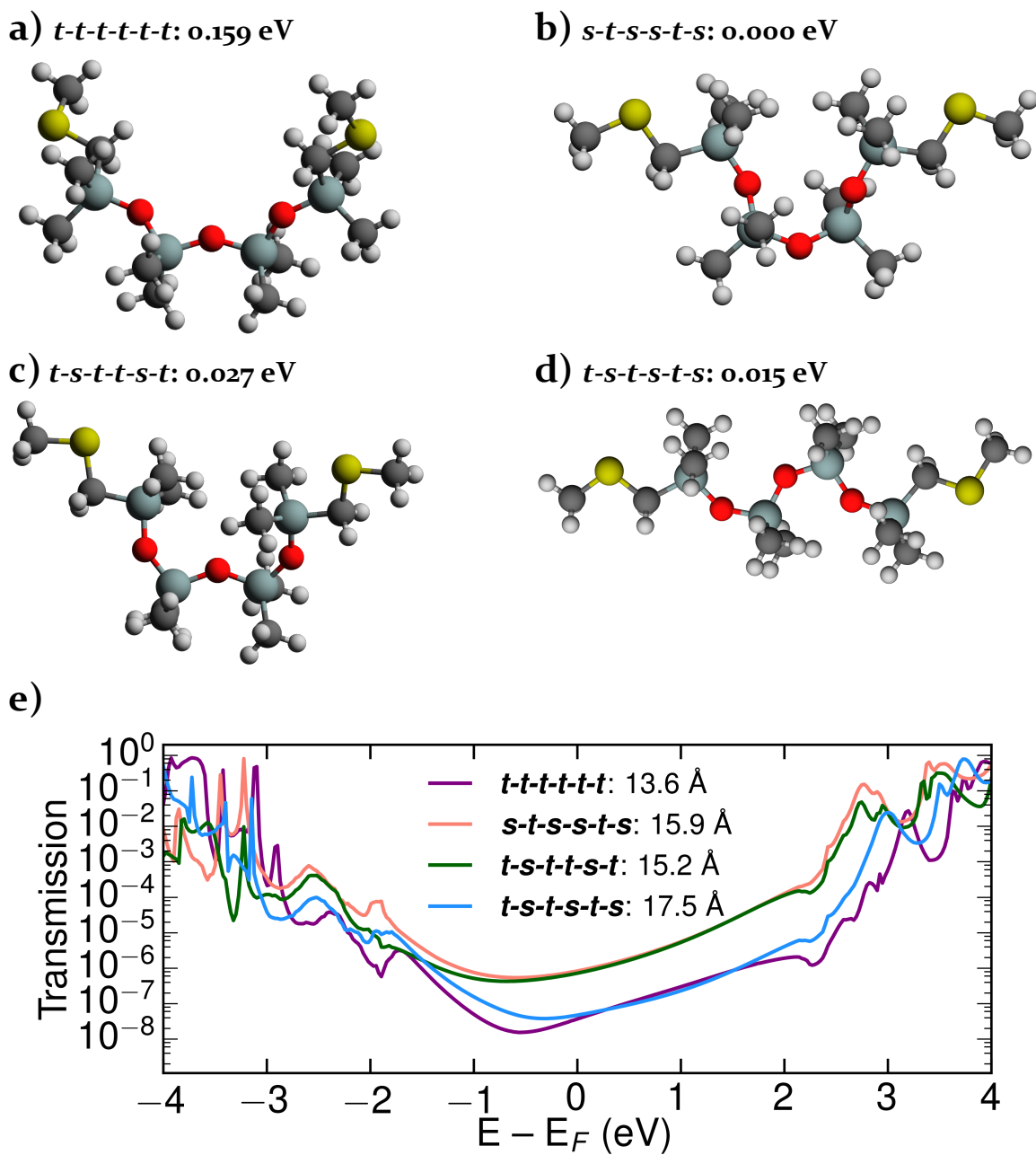


Figure S10. abcd) Optimized vacuum conformations of siloxane **3** and energy relative to the most stable conformation. e) transmission plotted semilogarithmically against energy. Junction tip-to-tip Au-Au length is listed.

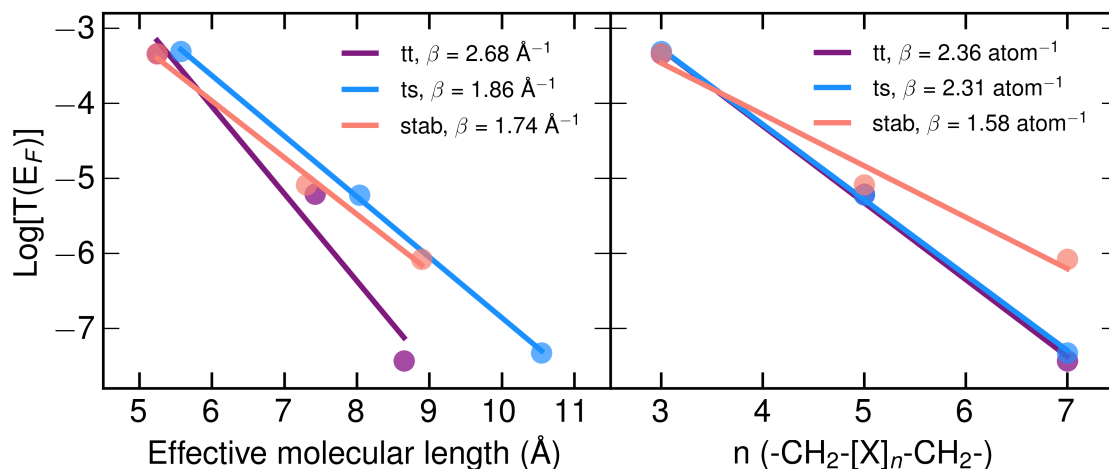


Figure S11. Logarithm of the transmission at the Fermi energy plotted against effective molecular length (left) and number of atoms in the backbone (right) for siloxanes. The plotted series of conformation are the all-*transoid*, alternating-*transoid-syn*, and the most stable conformations (*tt*, *tstt*, *stssts*). The exponential decay factors, β , are listed in the legend.

D: Alkoxane series and effect of conformational freedom

To probe whether the conformations with *syn*-dihedrals are part of the reason why the conductance decay is so exceptionally steep for siloxanes, we have made a small comparative study with the molecules examined in Wierzbinski *et al*¹³ and Xie *et al*.¹⁴ In those works the conductance of a series of oligoethers were compared to the equivalent alkanes. Here we have calculated the transmission for the equivalent series with methylthiomethyl linkers, as shown in the top panel of Figure S12. Furthermore, we have calculated the alkoxane series which is the equivalent carbon-based series to our siloxanes. In contrast to our siloxanes, these three series all-adopt all-*transoid* conformations. In the left panel of Figure S11, the transmission of the siloxane and three series is plotted against effective molecular length. In good agreement with the experimental studies, the exponential decay factor for the ether is only slightly bigger than that of the alkane series. The alkoxane further has a bigger decay constant, but still much smaller than that for the siloxane series. While the electronic delocalization through a carbon chain is systematically weakened by the incorporation of oxygen atoms, it is not nearly as weak as when oxygen atoms are incorporated in a silicon chain.

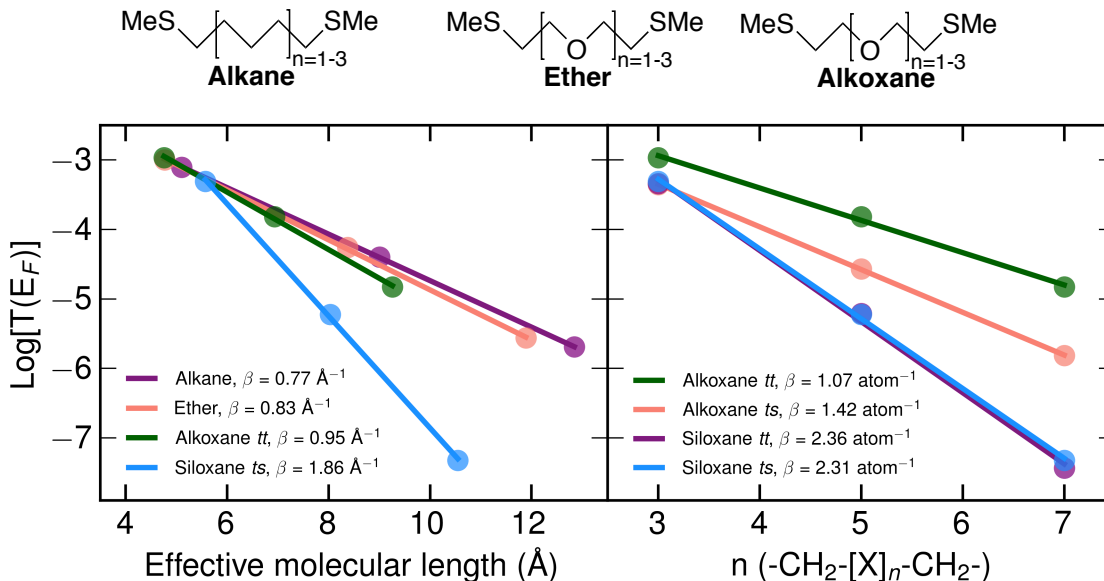


Figure S12. Top panel: Alkane, ether, and alkoane molecular series. Left panel: Logarithm of the transmission at the Fermi energy plotted against effective molecular length for the alkane and ether series of Wierzbinski *et al*¹³ and Xie *et al*¹⁴ and the alkoane all-*transoid* and siloxane alternating-*transoid-syn* series. Right panel: Logarithm of the transmission at the Fermi energy plotted against number of atoms in the backbone for the all-*transoid* and alternating-*transoid-syn* series of alkoane and siloxane. Alternating-*transoid-syn* of alkoane are not stable conformations and are therefore not optimized. The exponential decay factors, β , are listed in the legend.

Finally, we have manipulated the alkoane chain to have the same dihedrals as the alternating-*transoid-syn* series of the siloxanes, therefore C-O-C bond angles are 130° (the optimized bond angles are ~112°). These are not stable conformations of the alkoanes, and therefore were not optimized further. In the right panel of Figure S11 the transmission decays per atom of the all-*transoid* and alternating-*transoid-syn* series of alkoane are compared. While the siloxane series show very similar decay, the alkoane decay is notably higher with *syn* dihedrals in the backbone. Still the siloxane has a much steeper decay. From these calculations, it is clear that the dihedrals do not have a major effect on the exponential decay factor of siloxanes, and cannot fully account for the difference in decay between alkoanes and siloxanes. While our choice of conformation does change the exact number we report for the decay factor, it does not change the fact that the decay of siloxane is significantly larger than any decay constants previously reported for single-molecule conductance.

D: HOMO-LUMO gap and sulfur orbital splitting

Here we report the highest occupied molecular orbital-lowest unoccupied molecular orbital (HOMO-LUMO) gaps and sulfur orbital splitting of the molecules in vacuum. These are all based on the Kohn-Sham orbitals we obtain from the relatively simple DFT calculations using the methods (ASE-GPAW) as described in the manuscript. Therefore they should primarily be interpreted with regards to the transmission calculations that we have reported, which are calculated using the same methods and software. All orbitals are plotted using an isovalue of 0.02. We report the HOMO-LUMO gaps for the molecules with the terminal methyl groups in anti-configuration. As shown in Figure S13 for **C5**, the HOMO mainly has character of the sulfur p-orbitals. Therefore, we consider also the effective HOMO which has the character of carbon σ -orbitals as these are expected to be more relevant for electron transport. For siloxanes, the sub-HOMO orbitals can furthermore have strong oxygen lone-pair character, therefore we have not considered those as effective HOMOs for the siloxanes.

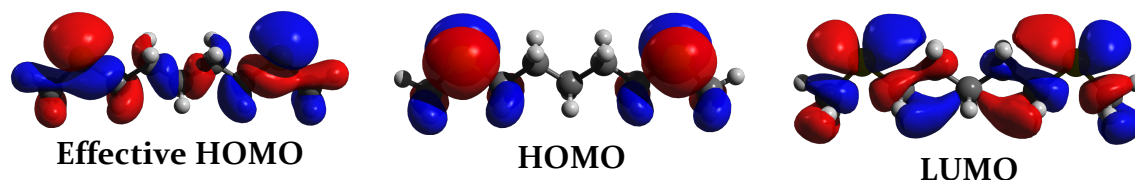


Figure S13. Effective HOMO, HOMO, and LUMO of **C5** with terminal methyl groups in anti-configuration.

As another measure of the electronic coupling through the molecular backbone, we report the sulfur orbital splitting for molecules with the terminal methyl groups in ortho-configuration. By symmetry, this allows the sulfur p-orbitals to mix with the carbon σ -orbitals and thereby they will split into bonding and antibonding combinations. This is visualized in Figure S14 for **C5**, where the HOMO-1 and HOMO are split by 0.092 eV (as listed in Table S1).



Figure S14. HOMO-1 and HOMO of **C5** with terminal methyl groups in ortho-configuration. These are essentially sulfur orbitals coupled through the molecular backbone.

In Table S1 the HOMO-LUMO gaps and sulfur orbital splittings are listed for select molecules of the alkane, silane, and siloxane series. The HOMO-LUMO gaps of alkanes is slightly bigger than that of the equivalent siloxanes, while the gap of silanes is considerably smaller. As a signature of σ -conjugation, the HOMO-LUMO gap becomes smaller with increasing length for silanes. For alkanes and siloxanes the gap is practically constant with increasing length and the electronic coupling through the molecules is expected to be weak.

The sulfur orbital splitting is generally consistent with the transmission decay. For silanes, the splitting is the largest and the decay is the slowest; for alkanes the splitting is smaller and the decay is faster; for siloxanes, the splitting is much smaller and the decay is even faster. Unfortunately, we cannot use this analysis on the alternating-*transoid-syn* series of the siloxanes, as sulfurs are required to be in chemically equivalent positions, i.e. there must be a symmetry operation that takes each sulfur p-orbital into the p-orbital of the other sulfur. For siloxane **3** this is (to good approximation) fulfilled for the *s-t-s-s-t-s* conformation. In agreement with the transmission, the orbital splitting is almost an order of magnitude higher than for the all-*transoid* conformation (see Figure S10).

Table S1. HOMO-LUMO gaps and sulfur orbital splitting calculated for all-*transoid* conformations of molecules in vacuum using DFT as described in the manuscript.

	HOMO-LUMO gap (eV)	Eff. HOMO-LUMO gap (eV)	S orbital splitting (eV)
C5	5.10	7.55	0.092
C7	5.14	7.57	0.039
C12	5.15	7.47	0.006
Si3	4.30	5.14	0.198
Si5	3.91	4.35	0.144
Si7	3.69	3.91	0.112
Siloxane 1	5.01	6.71	0.033
Siloxane 2	4.93	6.82	0.003
Siloxane 3	4.84	6.87	0.002
Siloxane 3 <i>s-t-s-s-t-s</i>	5.00	6.84	0.018

E: Complex band structure

The procedure used to calculate the complex band structure is given below:

- The unit cells for alkane, silane and siloxane were built by cutting a long molecule down to the smallest repeat unit as an initial guess, see Figure S15, except for the siloxane, which has four silicon and four oxygen atoms to resemble the molecules as much as possible.
- The unit cells were then optimized by constraining the transverse directions (x and y) but allowing the z vector to change.

The complex band structure was then calculated for the optimized unit cell, where the plots in Figure 3 show kz and $kappa$ in z-direction at $kx, ky = (0,0)$.

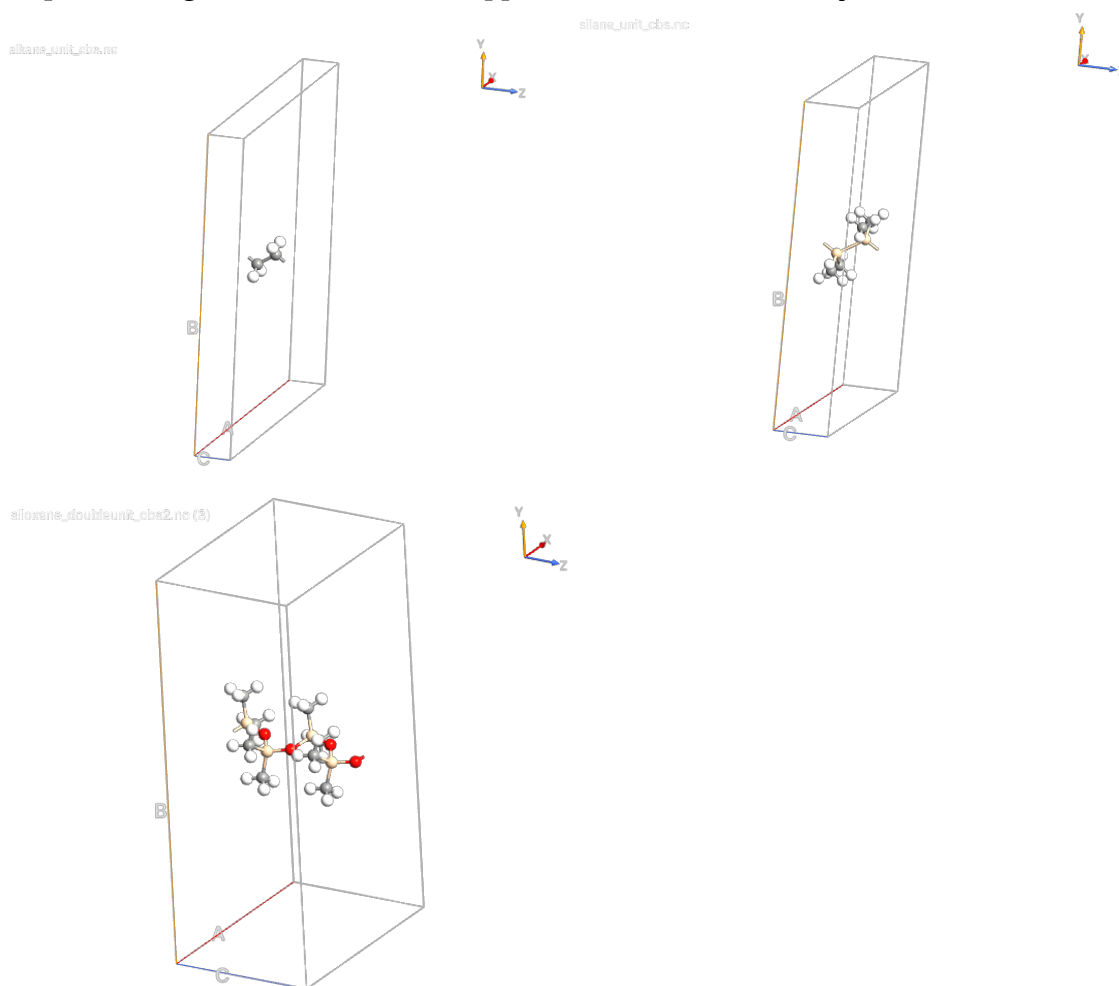


Figure S15. Unit cell of alkane, silane and siloxane, respectively.

Connection between interaction strength (hopping element) and onsite energies and decay constant β

We build a model of an infinite chain with alternating sites (a and b) to illustrate how onsite energies and hopping elements can influence the decay constant β . This model is a simple approximation of the Si-O electronegativity alternation in the siloxanes. The model is similar to the model in Tomfohr and Sankey *et al.*¹⁵

In the top panel of Figure S16 the hopping element t is varied while the onsite energies are constant. We see that large interaction strength gives large dispersion in the bands and weak interaction gives a small dispersion and large decay constant ($\sim 2|k_i|$).

In the bottom panel of Figure S15 we vary the difference in onsite energies e_a and e_b while keeping t constant. We find that when the two sites differ a lot in energy we also have low dispersion and high $|k_i|$ while similar onsite energies give larger dispersion and small $|k_i|$.

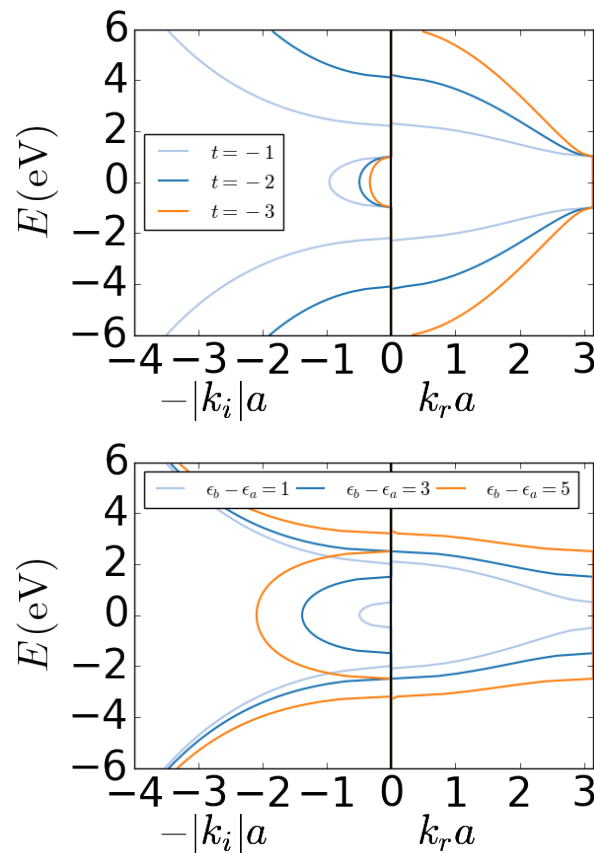


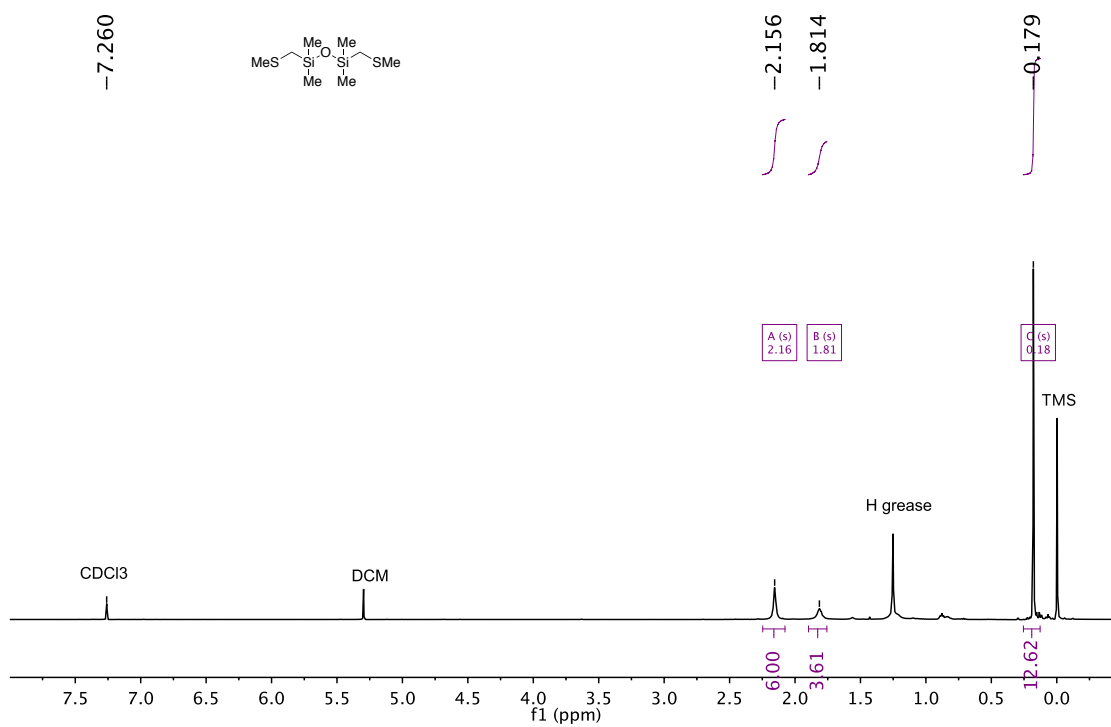
Figure S16. Complex band structure of an infinite chain of alternating sites. Top: the hopping element t is varied while the onsite energies are constant. Bottom:

The energy difference between the onsite energies is varied while keeping the hopping element constant.

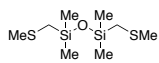
IV. NMR Spectra (^1H , ^{13}C , ^{29}Si):

$[\text{SiO}]_n$

^1H NMR (500 MHz, Chloroform-*d*) δ 2.16 (s, 6H), 1.81 (s, 4H), 0.18 (s, 12H).

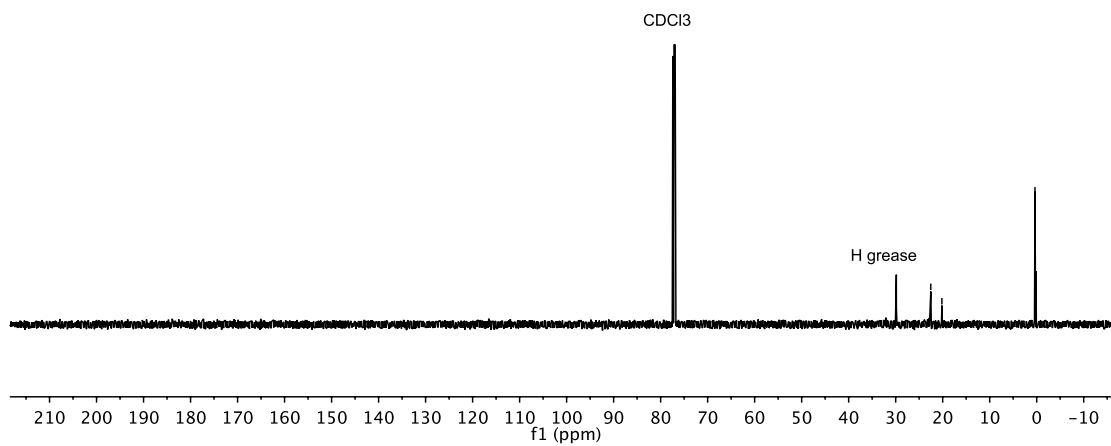


^{13}C NMR (126 MHz, CDCl_3) δ 22.53, 20.17, 0.37.

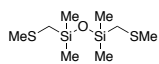


22.533
20.169

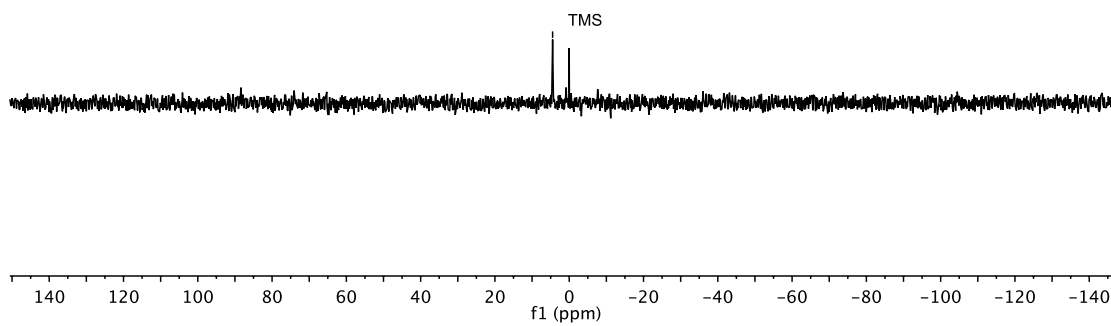
-0.366



^{29}Si NMR (60 MHz, CDCl_3) δ 4.48.

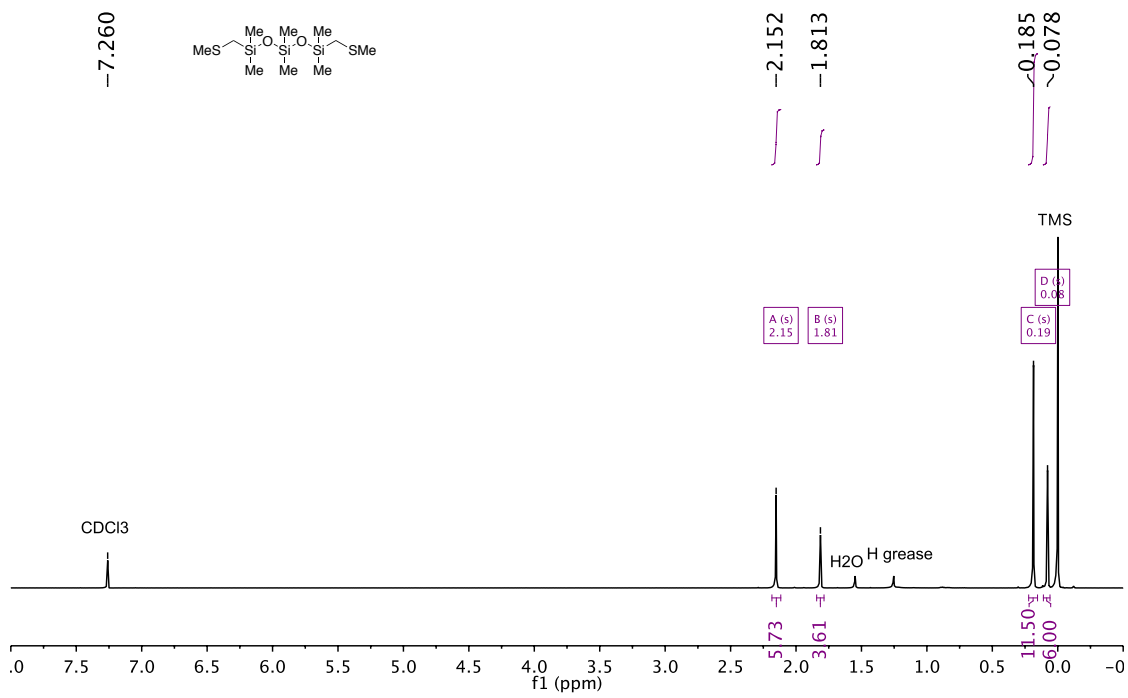


-4.475

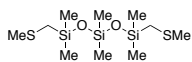


$[\text{SiO}]_2$

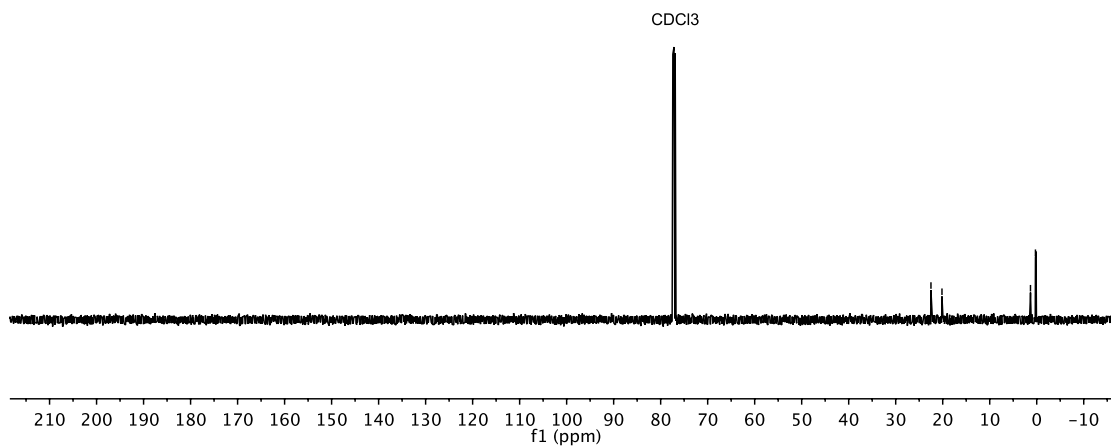
¹H NMR (500 MHz, Chloroform-*d*) δ 2.15 (s, 6H), 1.81 (s, 4H), 0.19 (s, 11H), 0.08 (s, 6H).



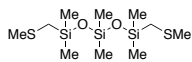
¹³C NMR (126 MHz, CDCl₃) δ 22.50, 20.16, 1.33, 0.27.



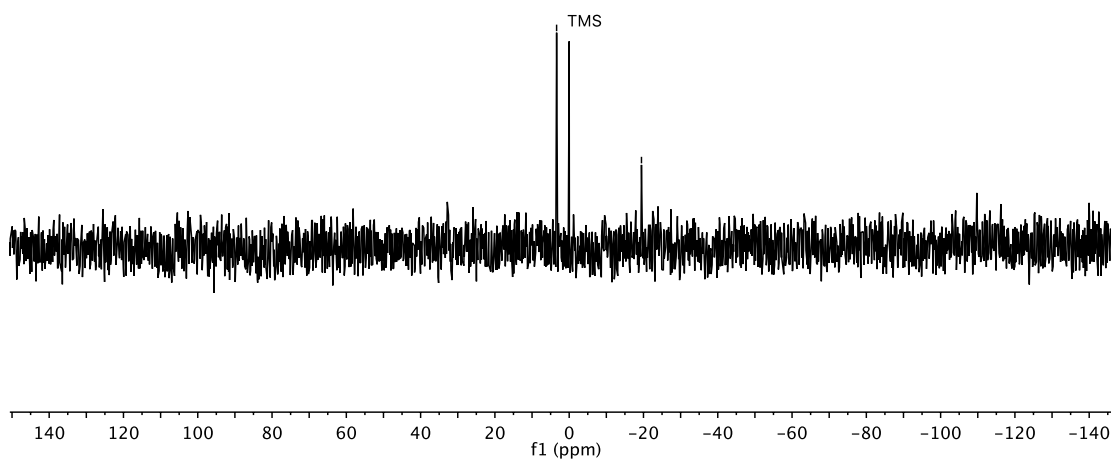
✓ 22.500
✓ 20.156
✓ 1.328
✓ 0.272



²⁹Si NMR (60 MHz, CDCl₃) δ 3.39, -19.46.

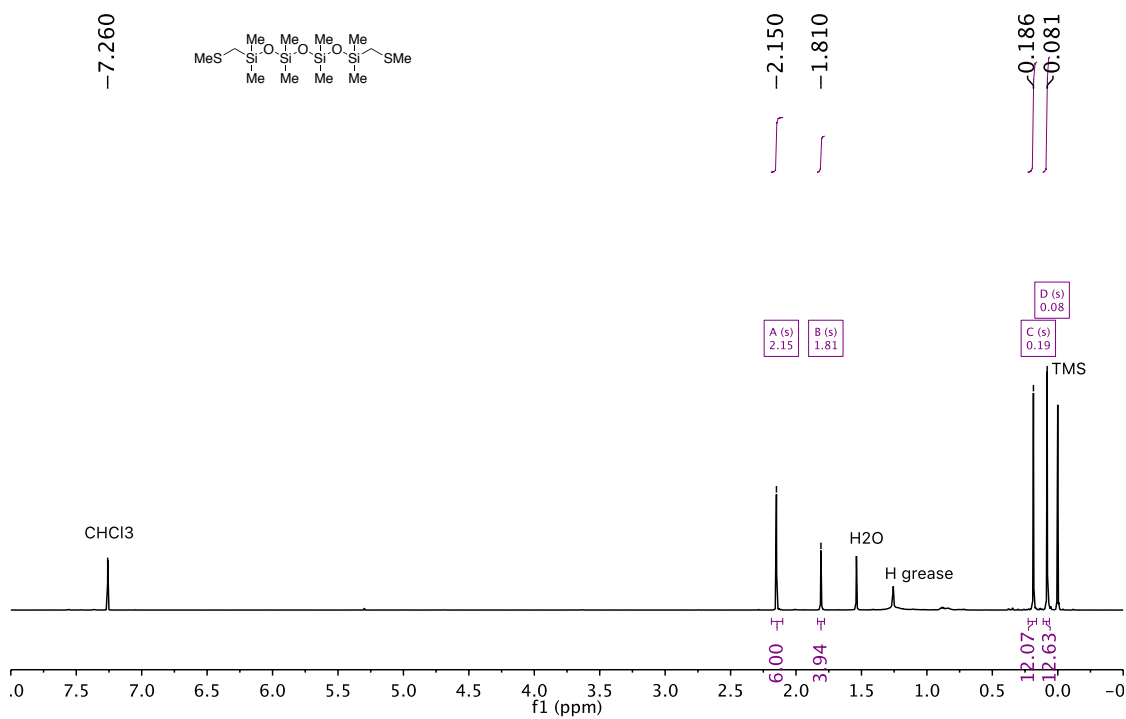


- 3.388
- -19.461

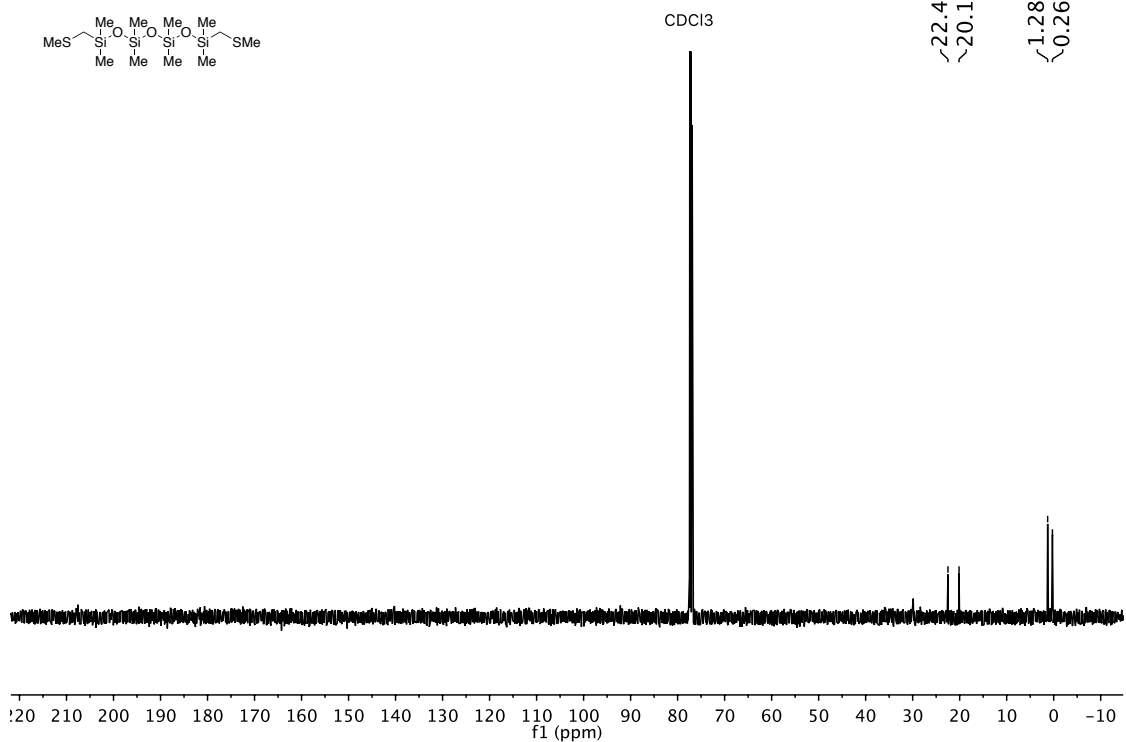


[SiO]₃

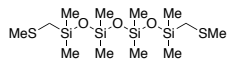
¹H NMR (500 MHz, Chloroform-*d*) δ 2.15 (s, 6H), 1.81 (s, 4H), 0.19 (s, 12H), 0.08 (s, 12H).



¹³C NMR (126 MHz, CDCl₃) δ 22.49, 20.13, 1.28, 0.27.

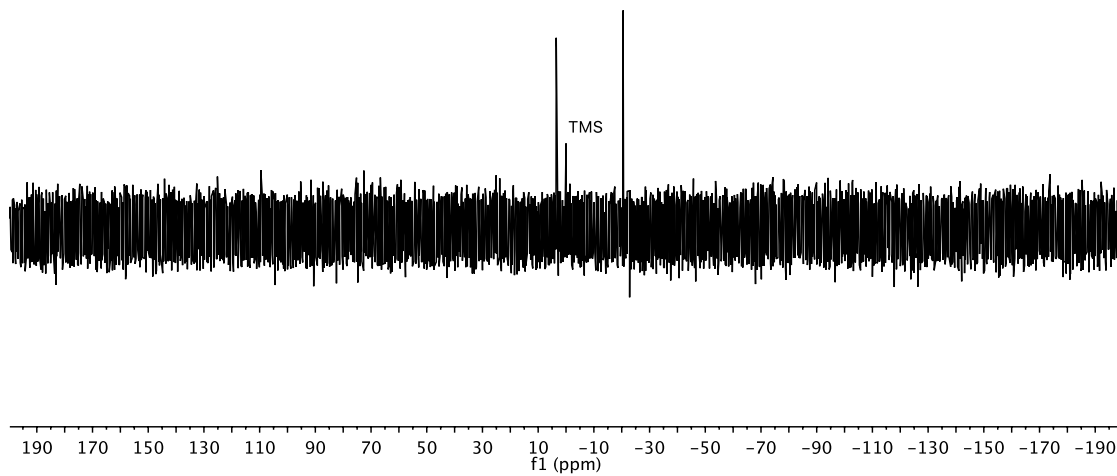


²⁹Si NMR (99 MHz, CDCl₃) δ 3.51, -20.49.



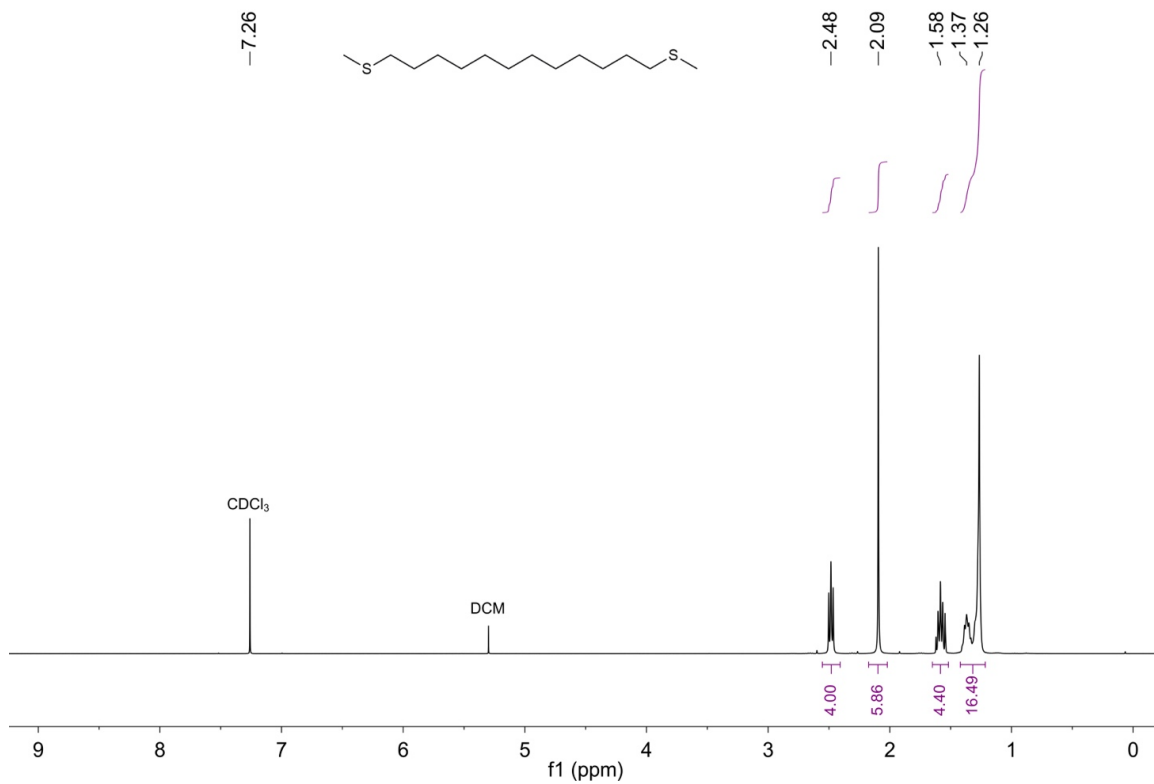
-3.513

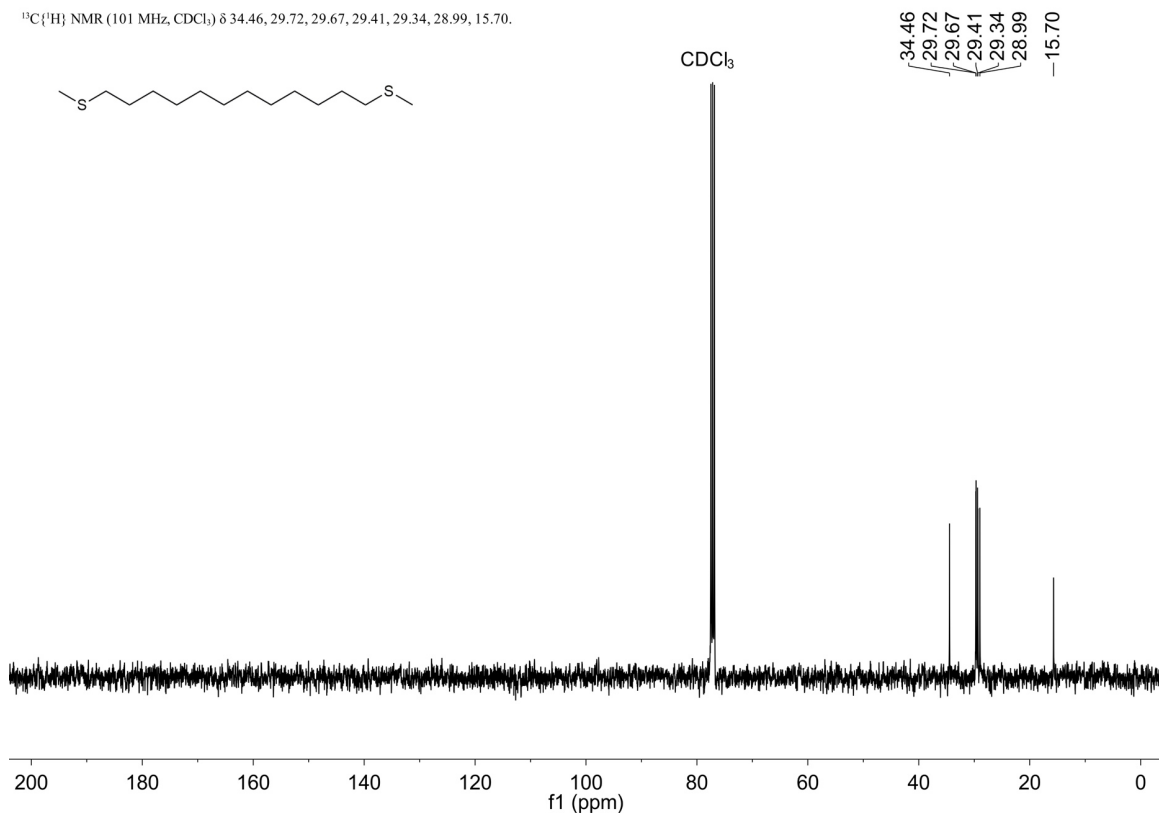
--20.492



C12

¹H NMR (400 MHz, CDCl₃) δ 2.48 (t, *J* = 7.4 Hz, 4H), 2.09 (s, 6H), 1.58 (m, 4H), 1.42-1.22 (m, 16H).





V. References

1. Su, T. A.; Li, H.; Steigerwald, M. L.; Venkataraman, L.; Nuckolls, C. *Nat. Chem.* **2015**, *7*, 215-220.
2. Li, H.; Su, T. A.; Zhang, V.; Steigerwald, M. L.; Nuckolls, C.; Venkataraman, L. *J. Am. Chem. Soc.* **2015**, *137*, 5028-33.
3. Michl, J.; West, R. *Acc. Chem. Res.* **2000**, *33*, 821-823.
4. Fogarty, H. A.; Casher, D. L.; Imhof, R.; Schepers, T.; Rooklin, D. W.; Michl, J. *Pure Appl. Chem.* **2003**, *75*, 999-1020.
5. Al Derzi, A. R.; Gregušová, A.; Runge, K.; Bartlett, R. J. *Int. J. Quantum Chem* **2008**, *108*, 2088-2096.
6. Weinhold, F.; West, R. *Organometallics* **2011**, *30*, 5815-5824.
7. Weinhold, F.; West, R. *J. Am. Chem. Soc.* **2013**, *135*, 5762-5767.
8. Moraru, I.-T.; Petrar, P. M.; Nemeş, G. *J. Chem. Phys. A* **2017**, *121*, 2515-2522.
9. Carteret, C.; Labrosse, A. *J Raman Spectrosc* **2010**, *41*, 996-1004.
10. Cypryk, M.; Gostyński, B. *J Mol Model* **2016**, *22*, 35.
11. Lupton, E. M.; Achenbach, F.; Weis, J.; Bräuchle, C.; Frank, I. *J. Chem. Phys. B* **2006**, *110*, 14557-14563.
12. Schwaderer, P.; Funk, E.; Achenbach, F.; Weis, J.; Bräuchle, C.; Michaelis, J. *Langmuir* **2008**, *24*, 1343-1349.

13. Wierzbinski, E.; Yin, X.; Werling, K.; Waldeck, D. H. *J. Chem. Phys. B* **2013**, *117*, 4431-4441.
14. Xie, Z.; Bâldea, I.; Oram, S.; Smith, C. E.; Frisbie, C. D. *ACS Nano* **2017**, *11*, 569-578.
15. Tomfohr, J. K.; Sankey, O. F. *Phys. Rev. B: Condens. Matter Mater. Phys.* **2002**, *65*, 245105.